

Corrosion Inhibitive Action of Tenofovir Disproxil Fumarate (TDF) on Low Carbon Steel in 1M HCl

M. M. Mohamed^{1,6,*}, B. M. Prasanna^{2*}, Narayana Hebbar³, Raiedahah Alsaiari¹, G. Banuprakash⁴, M. R. Jagadessh⁵, Moustafa A. Rizk^{1,6}

¹ Empty Quarter Research Unit, Department of Chemistry, College of science and art in Sharurah, Najran University, Sharurah, Saudi Arabia

² Department of Chemistry, Jain Institute of Technology, Davanagere, (Affiliated to Viswesaraya Technological University, Belagavi), Karnataka, India

³ Department of Chemistry, S. D. M. College, Ujire, Dakshina Kannada, Karnataka, India

⁴ Department of Chemistry, S. J. B. Institute of Technology, Bangalore, Karnataka, India

⁵ Department of Physics, Jain Institute of Technology, Davanagere, Karnataka, India

⁶ Department of Chemistry of Science faculty, Suez Canal University, Ismailia 41522, Egypt

*E-mail: mmmohammad@nu.edu.sa (M. M. Mohamed), drbmprasanna@gmail.com (B M Prasanna)

Received: 5 March 2021 / Accepted: 20 April 2021 / Published: 30 April 2021

The effect of Tenofovir Disproxil Fumarate (TDF) on the corrosion of low carbon steel in 1M HCl was investigated using theoretical and experimental methods at the temperature range of 303-333 K. The electrochemical measurements such as polarization and impedance measurements suggested that the inhibition efficiencies increase with the increasing concentrations of TDF and decreases with the increase in temperature. The electrochemical potentiodynamic polarization measurement reveals that the TDF acts as a mixed type corrosion inhibitor for steel in 1M HCl. The overall increasing inhibition efficiency of an inhibitor is attributed to the adsorption onto the steel surfaces from the bulk of the solution. The adsorption process is the most appropriate fit with the Langmuir adsorption isotherm model, and computed thermodynamic parameters were discussed. Thermodynamic parameters reveal that the TDF adsorbs spontaneously onto the metal surfaces and retards the corrosion by the chemisorption method. The activation parameters explain the effect of temperature on TDF inhibition efficiency for low carbon steel in 1M HCl. The quantum chemical parameters strengthen the experimental results and are also a good agreement between them. Scanning electron microscopic measurement provides a visual idea of creating a protective layer on steel surfaces, which reduces corrosion.

Keywords: Corrosion inhibitors; TDF; Electrochemical; SEM; Quantum

1. INTRODUCTION

Steel corrosion is a significant academic and industrial challenge of great importance due to its superior mechanical properties [1]. The steel undergoes corrosion due to exposure to acidic and alkaline media in chemical and allied industries. Therefore, the chloride, sulfate, and nitrate ions in aqueous media lead to accelerating the corrosion. Corrosion inhibitors are the most convenient and experimental method to control corrosion, especially in acid media [2].

In general, most of the corrosion inhibitors are organic heterocyclic compounds, consisting of electron-rich species such as nitrogen, oxygen, sulfur, and non-bonding π electrons in its heterocyclic ring system. The electron-rich species in inhibitor molecules bonding with the electron-deficient metal surface, by which adsorption takes place. The adsorption of inhibitor molecules over the metal surface retards the corrosion by forming a protective barrier at the metal/solution interface. Therefore, the reactive metal surface is passivated from the acid solution through the spontaneous adsorption process [3]. The adsorption of inhibitor molecules over metal surfaces depending upon the physio-chemical properties such as functional group, size, weight, structure, aromaticity of the molecule, the electron density of the donor atoms, steric factor, and nature of the donating electrons and their p-orbital. [4]. Most of the developed corrosion inhibitors for various metals in various corrosive media are toxic even they show good inhibitive capability. And also which are not stable to reduce corrosion at elevated temperatures. The planarity of the molecule influences the inhibition efficiency of the inhibitor for metal. As a result, drugs with a planar structure may be a promising inhibitor that has inspired us to use TDF drugs [5].

Tenofovir Disproxil Fumarate (TDF) is an antiretroviral drug used to prevent HIV-1 and AIDS infections. The IUPAC nomenclature of TDF is 9 - (R) - 2- (Bis(((isopropoxycarbonyl)oxy) phosphinyl) methoxy) propyl) adenine fumarate. The presence of electron-rich species such as nitrogen, oxygen, phosphorous, and π electrons in its heterocyclic ring system can favour its adsorption tendency on the metal surface, which provides the scope to this study. Herein, we investigate the corrosion inhibition study of TDF for soft-casting steel in 1M HCl media through gravimetric and electrochemical measurements. The quantum chemical calculations strengthen the results found experimentally, which correlates with experimental observations [6].

2. EXPERIMENTAL

2.1 Low carboning Steel

The commercially procured low carbon steel strips with the elemental composition of 0.05 % C, 0.32 % Mn, 0.019 % P, 0.041 % S, and the 99. 57 % Fe was used for all the corrosion experiments. The steel strips were designed mechanically with a dimension of $6 \times 1 \times 0.5 \text{ cm}^3$ have been used for weightless measurement. The same strip with an exposed area of 1 cm^2 (the rest of the surface insulated by epoxy resin) has been used for electrochemical measurements. All steel strips used for the

measurements were abraded using silicon carbide emery paper with the grade number of 80 up to 2000. After that, the strips were degreased with acetone followed by washing with deionized water.

2.2 Acidic Media

The acidic environment of 1M HCl was prepared by using AR-grade concentrated HCl. The concentrated HCl dissolved in deionized water to organize aggressive acidic media.

2.3 Corrosion Inhibitor

The organic heterocyclic compound TDF was selected as a corrosion inhibition study was procured by Sequent Scientific Limited, Mangalore. It is a white-coloured compound with a 635.5 g / mol molecular weight, which is easily soluble in 1M HCl to prepare inhibited samples in corrosion experiments. 250, 500, 750, 1000, 1250 mg of TDF dissolved in 1 litre of 1M HCl were used as inhibited samples. The molecular structure of TDF is as shown in Figure 1.

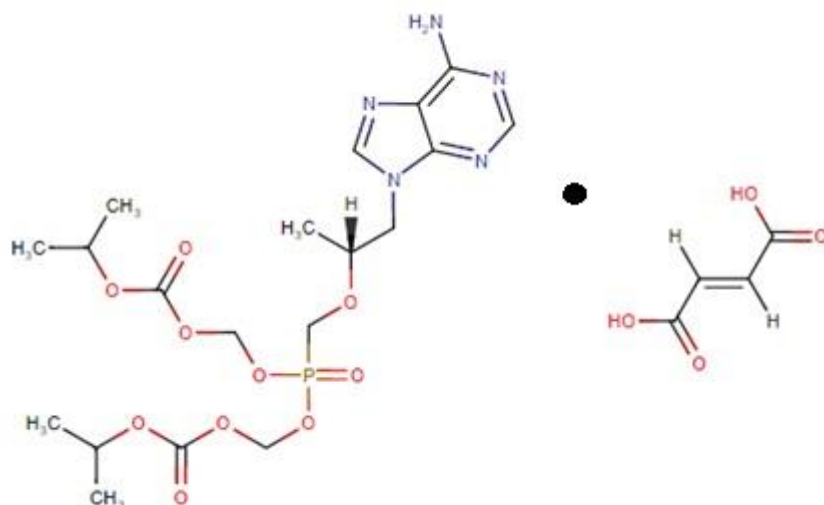


Figure 1. The molecular structure of TDF.

2.3 Weight Loss Measurement

Weight loss measurement was carried out by immersing steel strips in 1M HCl with various TDF concentrations. All the steel strips were taken out after the immersion of 4 hrs. Then these strips were washed with deionized water, dried at room temperature, and weighed by using an electronic balance (accuracy ± 0.1 mg). Triplicate experiments were conducted, and average values were reported. The corrosion rate and inhibition efficiency of the inhibitor calculated and discussed.

2.4 Potentiodynamic Polarization Measurement

The potentiodynamic polarization measurement for low carbon steel was recorded in CHI608D electrochemical workstation through the three-electrode assembly at a temperature range of 303 - 333 K. Typical three-electrode assembly consists of a low carbon steel strip as a working electrode, platinum electrode as an auxiliary electrode, and saturated Ag / AgCl electrode as a reference electrode. All the electrochemical measurements were carried out after 30 min immersion period for low carbon steel to attain steady open circuit potential (OCP). Under galvanostatic conditions, the potential-current curves for anodic and cathodic polarization values were measured at a scan rate of 2 mVs⁻¹. The inhibition efficiency and corrosion parameters were computed by Tafel extrapolation and discussed.

2.5 Electrochemical Impedance Spectroscopy (EIS) Measurement

The electrochemical impedance spectroscopic (EIS) measurements were recorded with a frequency range from 10 k Hz to 0.1 Hz at the AC amplitude of 5 mV. The inhibition efficiency and corrosion parameters were calculated by fitting an experimental curve to an electrical equivalent circuit.

2.6 Thermodynamic Considerations

The corrosion inhibition effect of inhibitors is attributed to the adsorption onto the metal surfaces from solutions [7]. To study the mode of adsorption of TDF molecules on low carbon steel surface in 1M HCl at different temperatures were made to fit EIS data into various adsorption isotherm models. The Langmuir adsorption isotherm model was the most appropriate fit by the experimental data from EIS measurement. Thermodynamic parameters were computed by using standard equations and discussed.

2.7 Activation Parameters

The effect of temperature on inhibition efficiency for low carbon steel in the absence and presence of TDF in 1M HCl at a temperature range of 303-333 K carried out by activation parameters. Therefore, the activation parameters were computed and discussed by fitting the corrosion rate values found by potentiodynamic polarization measurements.

2.8 Scanning Electronic Microscopic (SEM) Measurement

The surface morphology of steel specimens was studied by immersing steel strips in the absence and presence of inhibitor in 1M HCl for about 4 hrs immersion period was done by SEM micrographs. The SEM micrographs were obtained from JEOL JSM – 840A scanning microscopy by an accelerated beam with an energy of 20 kV.

2.7 Quantum Chemical Calculations

The quantum chemical calculations for the TDF molecule were performed under the gas phase using the Parametric Method 3 (PM3) method. The Polak-Rieberre algorithm computed the quantum parameters because of its accuracy. The root mean square gradient energy parameters were kept at 0.05 kcal/mol, with the convergence limit being 0.05. These computations were carried out using a professional software Hyperchem 7.5 package program (Hypercube Inc., Florida, 2003).

3. RESULT AND DISCUSSION

3.1 Weight Loss Measurements

The inhibition efficiency for low carbon steel in 1M HCl in the absence and presence of TDF in 1M HCl at a temperature of 303 K carried by weight loss measurement with an immersion period of 4 hrs. The inhibition efficiency (η_w) of TDF found from weight loss measurement is calculated by the following expression,

$$\eta_w = \frac{W^o - W}{W^o} \times 100$$

(1)

Where W^o and W are weight loss of low carbon steel in the absence and presence of TDF in 1M HCl, respectively. The following equation measured the corrosion rate (ρ) of steel as,

$$\rho = \frac{W^o - W}{ST} \times 100$$

(2)

Here, S and T are the surface area of low carbon steel strip and immersion time in hrs, respectively. The corrosion parameters obtained by weight loss measurement were reported in Table 1.

Table 1. The corrosion parameters obtained by weight loss measurement for low carbon steel in the absence and presence of various TDF concentrations in 1M HCl at the temperature range of 303-333 K.

Concentration of TDF	Corrosion Rate ρ (mpy)	Inhibition Efficiency η_w (%)
0	124.24	-
250	28.84	76.79
500	24.04	80.65
750	19.82	84.04
1000	15.22	87.74
1250	10.34	91.67

The results suggested that the inhibition efficiency increases with the increasing TDF concentration in 1M HCl due to the formation of a protective barrier at the metal/solution interface

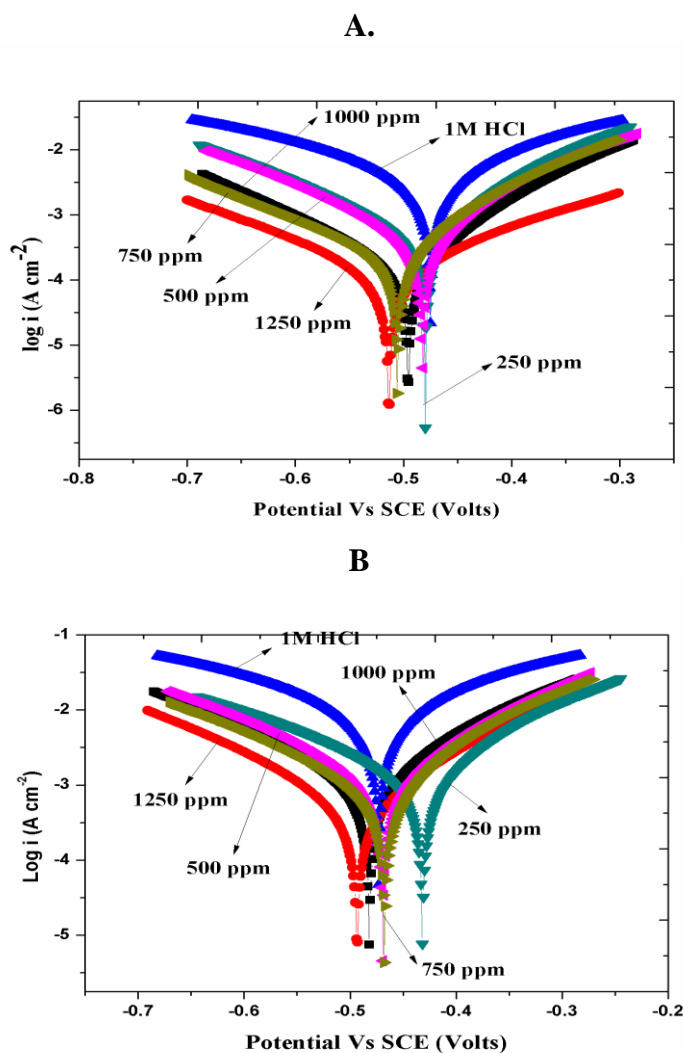
through adsorption of TDF molecules onto the surface of low carbon steel in 1M HCl [8]. The inhibition efficiency was found as 91.67 % for 1250 ppm of TDF in 1M HCl reveals that the TDF acts as a good corrosion inhibitor for low carbon steel.

3.2. Potentiodynamic Polarization Measurements

The potentiodynamic polarization measurements were carried out for low carbon steel in the absence and presence of various TDF concentrations in 1M HCl at a temperature range of 303-333 K, resulting in potential current curves in Figure 2. After that, computed corrosion parameters such as corrosion potential (E_{corr}), corrosion current density (i_{corr}), corrosion rate (v), and the inhibition efficiency (η_p) were reported in Table 2. The following equation calculated the inhibition efficiency of TDF,

$$\eta_p = \frac{i_{corr}^o - i_{corr}}{i_{corr}^o} \times 100 \tag{3}$$

Where i_{corr}^o and i_{corr} are the corrosion current densities for low carbon steel in the absence and presence of inhibitor in 1M HCl, respectively.



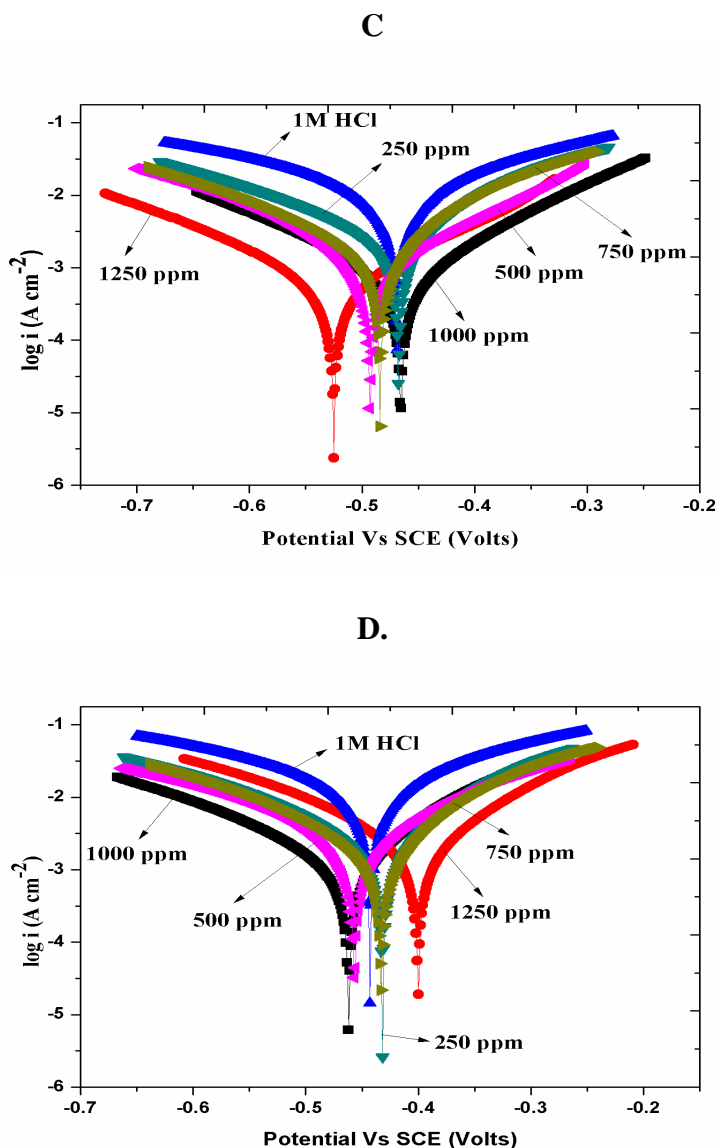


Figure 2. The potentiodynamic polarization plots of low carbon steel in the absence and presence of different concentrations of TDF in 1M HCl at a temperature of (A) 303 K (B) 313 K (C) 323 K (D) 333 K.

The results shown in Table 2 suggested that a decreasing corrosion current density (i_{corr}) with the increasing TDF concentration in 1M HCl was observed. The decreasing corrosion current density is attributed to the adsorption of inhibitor molecules onto the metal surfaces from the bulk of the solution, which is also because of the formation of passivation of metal surfaces by forming a protective barrier at the metal/solution interface. The inhibition efficiency of TDF was found as 92.84 % at its concentration of 1250 ppm up to the increasing temperature of 333 K. In general, the corrosion rate of the metal decreases with increasing temperature. Hence, the inhibitive capability of the inhibitor is also not effective due to the depletion of the adsorbed protective layer [9]. However, for TDF, the inhibition efficiency increased up to the temperature up to 333 K due to the higher in its adsorption.

The small displacement of corrosion potential (E_{corr}) value of the inhibited solution for the blank (1M HCl) is 61 mV. It is less than ± 85 mV shows that the TDF acts as a mixed type corrosion inhibitor

[10]. The mixed type inhibitor retards the corrosion by slowdowns either anodic or cathodic reactions, which causes the corrosion. Meanwhile, the decreasing corrosion rate (v) indicates the TDF forms a protective layer on steel surface in aggressive acidic media.

Table 2. The corrosion parameters obtained by potentiodynamic polarization measurements for low carbon steel in the absence and presence of different TDF concentrations in 1M HCl at the temperature range of 303-333 K.

Temperature (K)	Concentration of TDF (ppm)	Corrosion Potential , E_{corr} (V)	Corrosion Current Density i_{corr} (A cm ⁻²)	Corrosion Rate, v (mpy)	Inhibition Efficiency η_p (%)
303	Blank	-0.473	0.436	85.34	-
	250	-0.432	0.153	20.31	64.90
	500	-0.469	0.086	12.22	80.27
	750	-0.468	0.059	10.52	86.46
	1000	-0.493	0.054	8.94	87.61
	1250	-0.482	0.052	6.49	88.07
313	Blank	-0.475	0.177	99.50	-
	250	-0.480	0.091	24.30	48.58
	500	-0.482	0.079	17.82	55.36
	750	-0.506	0.051	15.53	71.18
	1000	-0.529	0.024	14.19	86.44
	1250	-0.513	0.019	10.08	89.26
323	Blank	-0.500	0.582	115.59	-
	250	-0.469	0.144	41.52	75.25
	500	-0.466	0.141	35.52	75.77
	750	-0.465	0.128	19.92	78.00
	1000	-0.468	0.104	18.32	82.13
	1250	-0.493	0.057	17.68	90.20
333	Blank	-0.443	0.694	139.71	-
	250	-0.502	0.141	73.32	79.68
	500	-0.432	0.111	45.22	84.00
	750	-0.484	0.110	27.62	84.14
	1000	-0.433	0.101	21.71	85.44
	1250	-0.400	0.064	21.51	90.77

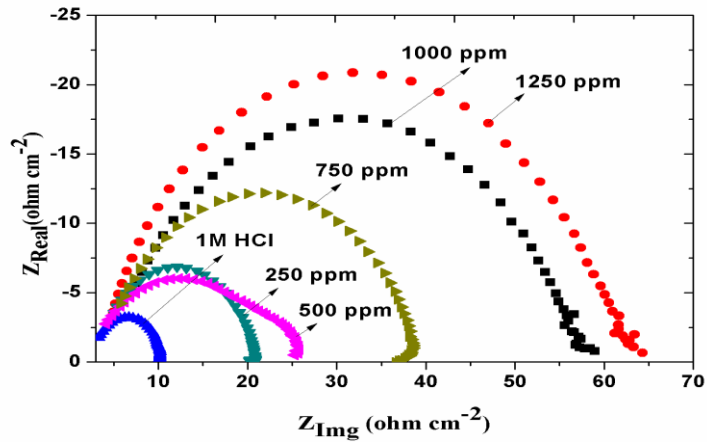
3.3. Electrochemical Impedance Spectroscopic (EIS) Measurements

Figure 3 is the EIS (Nyquist) spectra for low carbon steel in the absence and presence of different concentrations of TDF in 1M HCl at a temperature of 303-333 K. The EIS data from experimental spectra curves parameters were fit into a suitable electrical equivalent circuit as shown in Figure 4. The computed results were reported in Table 3. The polarization resistance (R_p) described as the diameter of the arc on the Nyquist plot and the inhibition efficiency (η_z) was calculated by the following expression,

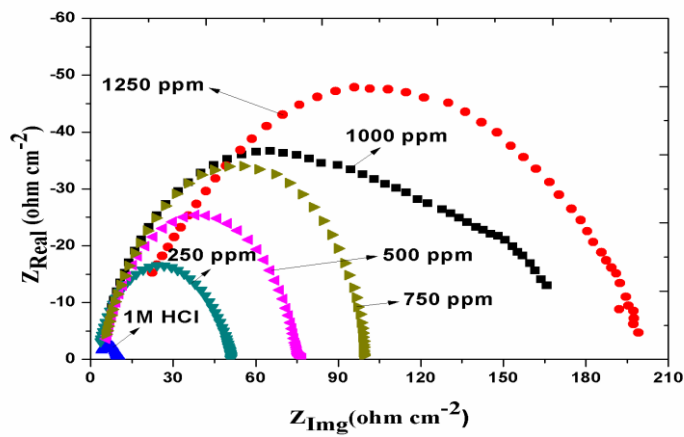
$$\eta_z = \frac{R_p - R_p^o}{R_p} \times 100 \tag{4}$$

R_p and R_p^0 are the polarization resistances in the absence and presence of different TDF concentrations in 1M HCl. The sample experimental curve is exactly matched with a curve obtained using an electrical equivalent circuit shown in Figure 5 for low carbon steel surface in the presence of 1250 ppm concentration of TDF in 1M HCl.

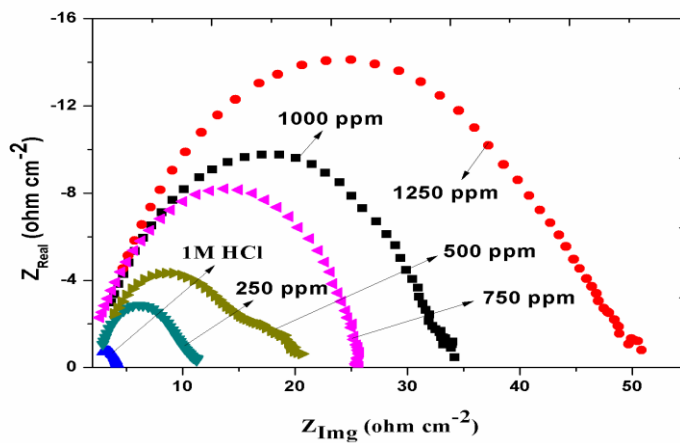
A



B



C



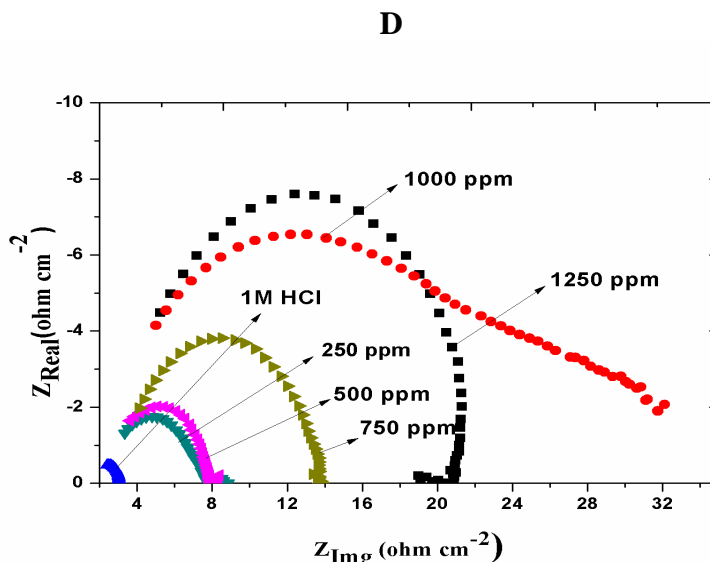
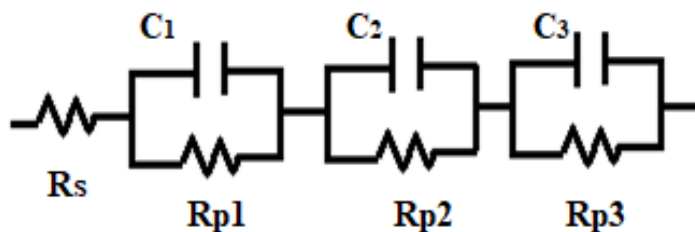


Figure 3. Nyquist plots for low carboning steel in the absence and presence of various concentrations of TDF in 1M HCl at (A)303 K (B) 313 K (C) 323 K (D) 333 K.



Where R_s = Solution resistance, R_{p1} , R_{p2} , R_{p3} = Polarization resistances, C_1 , C_2 , C_3 = Capacitances

Figure 4. The electrical equivalent circuit is used to interpret the results of the EIS.

Table 3: The corrosion parameters obtained by EIS measurement for low carbon steel in the absence and presence of different TDF concentrations in 1M HCl at a temperature range of 303-333 K.

Temperature (K)	Concentration of TDF (ppm)	Polarization Resistant, R_p ($\Omega \text{ cm}^2$)	Double-layer Capacitance, C_{dl}	Inhibition Efficiency, η_z (%)	Surface Coverage, θ
303	Blank	8.27	3474	-	-
	250	17.32	2398	52.25	0.522
	500	22.15	1716	62.66	0.626
	750	33.94	1161	75.63	0.756
	1000	50.84	1105	83.73	0.837
	1250	57.41	798	85.59	0.855
313	Blank	6.95	944	-	-
	250	46.95	692	85.19	0.851
	500	69.09	593	89.94	0.899
	750	93.54	326	92.57	0.925
	1000	152.06	287	95.42	0.954
	1250	173.55	274	95.99	0.959

323	Blank	2.12	4377	-	-
	250	8.41	4145	74.79	0.747
	500	23.51	2149	90.98	0.909
	750	16.36	1237	87.04	0.870
	1000	30.00	820	92.93	0.929
	1250	44.90	717	95.27	0.952
333	Blank	1.22	8169	-	-
	250	5.26	7453	76.80	0.768
	500	5.30	6290	76.98	0.769
	750	10.31	5194	88.16	0.881
	1000	20.97	4455	94.18	0.941
	1250	27.21	3906	95.51	0.955

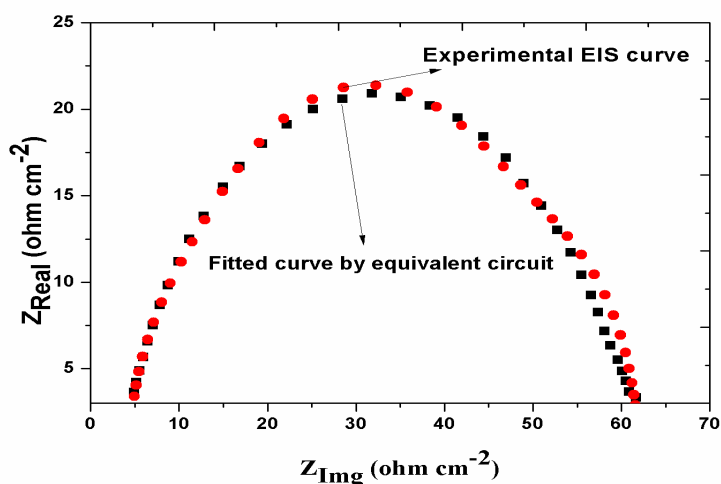
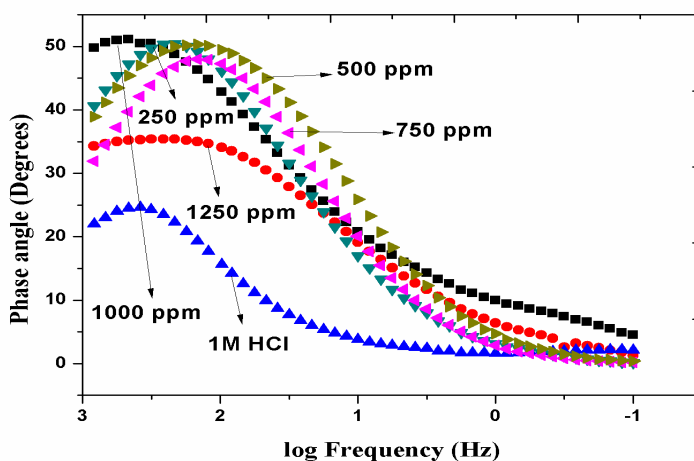


Figure 5. An experimental curve was fitted using a curve found by applying the electrical equivalent (Figure 4) circuit.

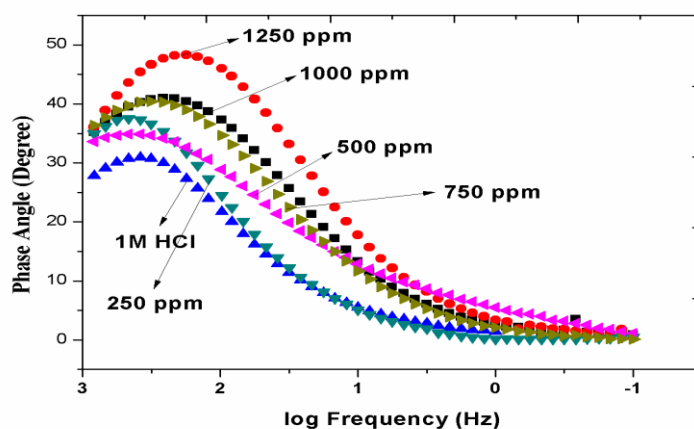
The EIS measurement results from Table 3 reveal that the R_p values increased with the increasing concentrations of TDF in 1M HCl. However, even though they have a semi-circular appearance, the capacitive loops are depressed with centres under the real axis. Generally, the semicircle diameter for the Nyquist plot is described as polarization resistance (R_p). The size of the semicircle with the inhibitor concentration reflects the inhibition efficiency of an inhibitor. The semicircle pattern deviation The inhibition efficiency of TDF was found by EIS measurement 95.20 % at its concentration of 1250 ppm up to the increasing temperature of 333 K. The double-layer capacitance (C_{dl}) values decreases gradually with the addition of TDF in 1M HCl, suggested that there is a decrease in the local dielectric constant or an increase in the thickness of the electrical double layer. As a result, a protective barrier is formed at the metal/solution interface, which retards the corrosion by adsorption. The results found by EIS measurement nearest to the results found by weight loss and potentiodynamic polarization measurements. EIS measurement also suggested that the TDF is a good corrosion inhibitor for low carbon steel in 1M HCl.

The Bode phase plots were plotted at OCP for low carbon steel in the absence and presence of TDF in 1M HCl, as shown in Figure 6. The phase angle increases with the increasing concentration of TDF in 1M HCl. The polarization resistance (R_p) is described as the difference between the high frequency (HF) and the low frequency (LF) limit in the bode plot. Thus, the polarization resistance is associated with the dissolution and passivation processes occurring at the metal/solution interface. With the increasing TDF concentration up to its critical concentration, the difference between the HF and LF for the absence and presence of inhibitor sample bode plot system increases. The increase in phase angle with an increase in TDF concentrations may be attributed to decreased capacitive behaviour at the metal surface due to reduced metal dissolution rate [12].

A



B.



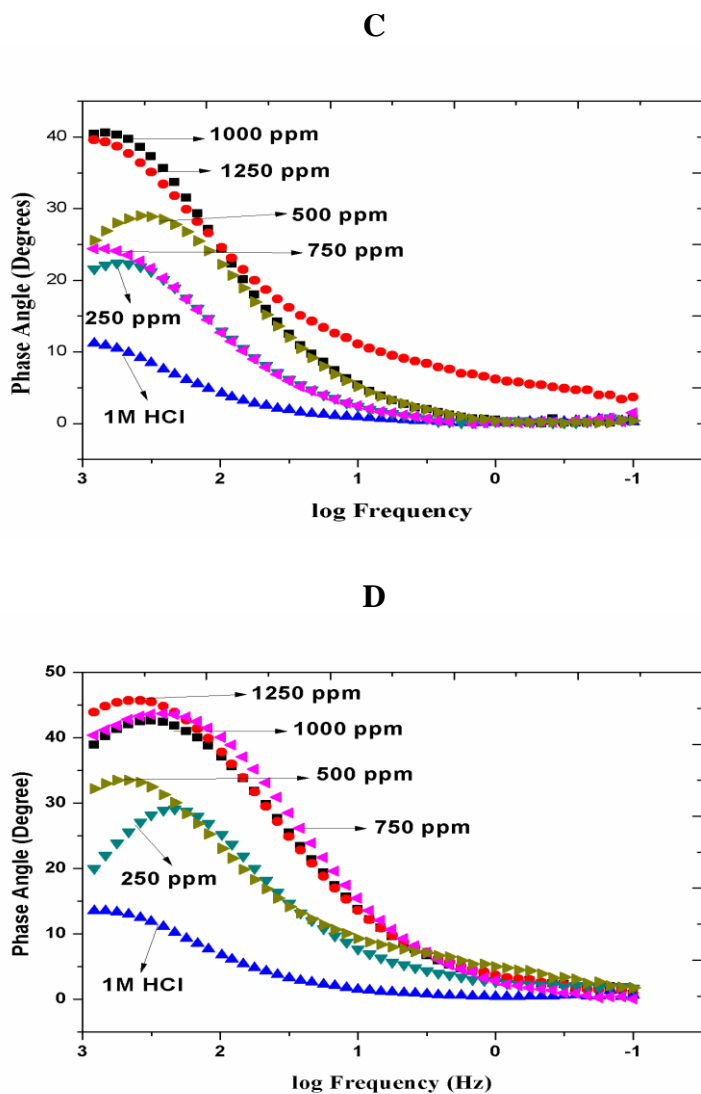


Figure 6. Bode plots for low carbon steel in the absence and presence of different concentrations of TDF in 1M HCl at a temperature of (A)303 K (B) 313 K (C) 323 K (D) 333 K.

3.4 Thermodynamic Parameters

EIS measurements were conducted to find out surface coverage (θ) values as shown in Table 3 for low carbon steel at various concentrations of TDF in 1M HCl at a temperature range of 303-333 K. The surface coverage values help to understand the corrosion inhibition mechanism with the adsorption behaviour of the inhibitor molecules on the metal surface. Therefore, the θ values explain the mode and kinetics of the adsorption by fitting a satiable adsorption isotherm model. The Langmuir adsorption isotherm model was the best fit for our experimental results, as shown in Figure 7.

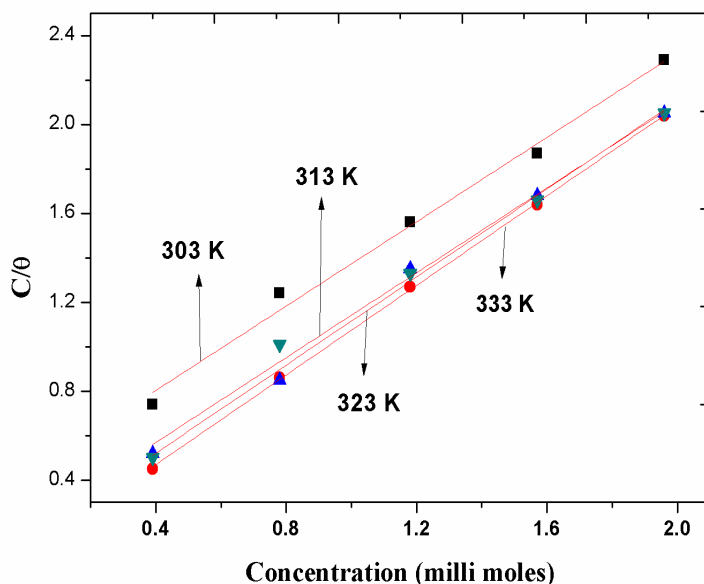


Figure 7. Langmuir adsorption isotherm of TDF in 1M HCl on low carbon steel at the temperature range of 303-333 K.

According to the Langmuir isotherm for monolayer adsorption is given by the following equation as

$$\frac{C}{\theta} = \frac{1}{K_{ads}} + C \tag{5}$$

K_{ads} is the equilibrium constant for adsorption, C is the concentration of inhibitor and θ is the degree of surface coverage. Plot a graph of inhibitor concentration (millimoles) against C / θ , as a result, to form a straight line. The intercept values were used to calculate the K_{ads} . After that, the standard free energy change of adsorption (ΔG^0_{ads}) were measured by using the following expression,

$$\Delta G^0_{ads} = -\ln(K_{ads} \times 55.5) \times R \times T \tag{6}$$

R is the ideal gas constant with the value of 8.314 J/mol/K, T is the absolute temperature, and the numerical value of 55.5 is the molar concentration of water in the sample. All calculated values of K_{ads} and ΔG^0_{ads} were reported in Table 4.

Table 4. Thermodynamic parameters for low carbon steel in the absence and presence of different TDF concentrations in 1M HCl at the temperature range of 303-333 K.

Temperature (K)	Equilibrium Constant, K_{ads} (kJ/mol)	Standard Free Energy Change, ΔG^0_{ads} (kJ/mol)	Standard Enthalpy Change, ΔH^0_{ads} (kJ/mol)	Standard Entropy Change, ΔS^0_{ads} (J/mol/K)
303	14925	-29.68	-76.11	-0.153
313	8000	-33.83	-76.11	-0.135
323	5319	-34.87	-76.11	-0.127
333	2358	-35.46	-76.11	-0.122

The values of K_{ads} describe the strong adsorption of inhibitor molecules on the metal surface from the bulk of the solution. A higher value of K_{ads} indicates strong adsorption of inhibitor molecules, resulting in high inhibition efficiency. The magnitude of ΔG^0_{ads} approximately -20 kJ mol^{-1} or lower values of ΔG^0_{ads} consistent with physisorption, and it is approximately -40 kJ mol^{-1} or higher is associated with chemisorption. Therefore, earlier researchers reported the importance of ΔG^0_{ads} lie in between -20 kJ mol^{-1} to -40 kJ mol^{-1} indicates that the adsorption of inhibitor process through the combination of both physisorption and chemisorption. In our study, the values of ΔG^0_{ads} were lies in between -20 kJ mol^{-1} to -40 kJ mol^{-1} but slightly reached towards -40 kJ mol^{-1} , suggested that the TDF adsorbed onto the metal surface through the combination of physisorption and chemisorption but predominantly because of chemisorption. The negative sign of the ΔG^0_{ads} value indicates the spontaneous adsorption of TDF molecules onto the metal surface from 1M HCl. After that, the enthalpy of adsorption (ΔH^0_{ads}) and entropy of adsorption (ΔS^0_{ads}) can be measured by the following Gibb's Helmholtz equation [13],

$$\left(\frac{\partial G/T}{\partial T} \right)_P = -\frac{H}{T^2} \quad (7)$$

The above mentioned Gibb's Helmholtz equation rearranged as [14],

$$\Delta S^0_{ads} = \frac{(\Delta H^0_{ads} - \Delta G^0_{ads})}{T} \quad (8)$$

Figure 8 is a plot of $\Delta G^0_{ads} / T$ against $1000 / T$, resulting in a straight line. The enthalpy of adsorption (ΔH^0_{ads}) was calculated by the straight-line intercept value, which describes the adsorption due to either an exothermic or an endothermic. Hence, the sign of ΔH^0_{ads} is +ve, the adsorption process is endothermic, and if it is -ve, the adsorption process is exothermic [15].

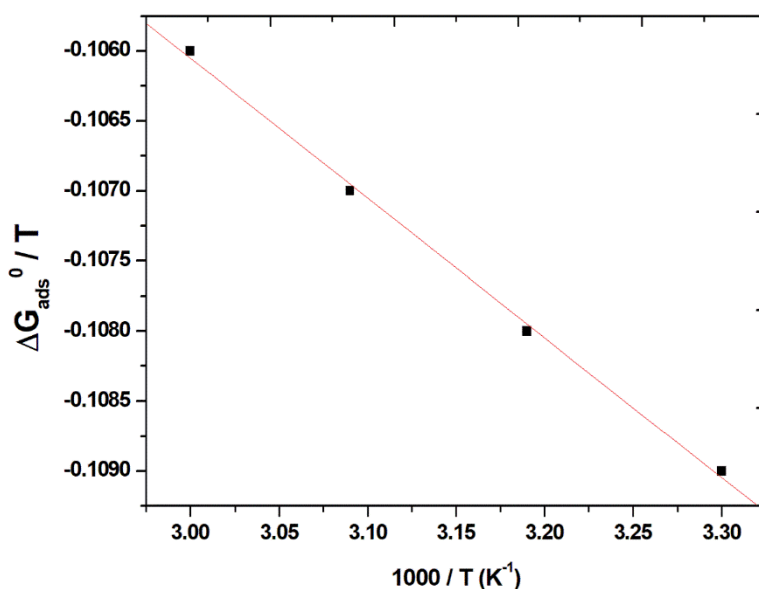


Figure 8. Graph of $1000 / T$ against $\Delta G_{\text{ads}}^0 / T$.

Generally, the value of enthalpy of adsorption (ΔH_{ads}^0) is approximately or less than 40 kJ/mol, the adsorption of inhibitor attributed because of physisorption and around and greater than 100 kJ/mol, the adsorption takes place through chemisorption. The current study consists of the value of ΔH_{ads}^0 is –ve sign suggested that the adsorption is exothermic reaction and magnitude is -76.11 kJ/mol, which is close towards -100 kJ/mol suggested that the adsorption mode is chemisorption. A +ve sign of entropy of adsorption (ΔS_{ads}^0) indicated that randomness increases at the metal/solution interface, which results in the adsorption of inhibitor molecules onto the surface of the metal. This increase in disorder is caused by an increase in the number of water molecules desorbed from the metal surface by inhibitor molecules [16].

3.5 Activation Parameters

The effect of temperature on inhibition efficiency of the inhibitor has a significant corrosion rate for the metals. The rate of corrosion increases with the increasing temperature. Because increasing temperature decreases the hydrogen overvoltage, which causes the increasing corrosion rate in acidic media. Usually, the mechanism of corrosion can be expressed by the Arrhenius equation as,

$$\ln v_{\text{Corr}} = \ln A - \frac{E_a^*}{RT} \quad (9)$$

Where v_{Corr} is the corrosion rate, E_a is the activation energy for the corrosion, R is the ideal gas constant, T is the absolute temperature, and A is Arrhenius pre-exponential factor. The Arrhenius plot of $\ln v_{\text{Corr}}$ against $1000 / T$ results straight line with slope equal to $-E_a / R$ and the intercept of $\ln A$ as shown in Figure 9. The calculated values of E_a and A were reported in Table 5.

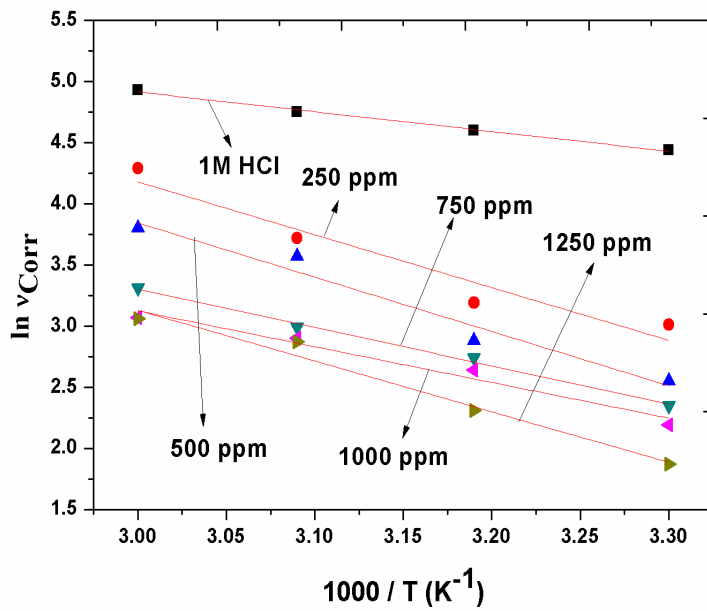


Figure 9. Arrhenius plot of $\ln v_{corr}$ against $1000 / T$

Table 5: Activation parameters for low carbon steel in the absence and presence of various TDF concentrations in 1M HCl at the temperature range of 303-333 K.

Concentration of TDF (ppm)	Activation Energy, E_a^* (kJ mol ⁻¹)	Arrhenius Pre-exponential Factor, A (g cm ⁻² h ⁻¹)	Enthalpy of adsorption, ΔH^* (kJ mol ⁻¹)	The entropy of Adsorption, ΔS^* (J mol ⁻¹ K ⁻¹)
Blank	13.18	56.23×10^8	10.89	-23.86
250	35.91	13.80×10^{16}	33.42	-16.48
500	36.91	14.45×10^{16}	35.91	-15.89
750	26.02	48.97×10^{11}	23.77	-20.83
1000	21.78	77.62×10^{10}	21.78	-21.72
1250	34.41	36.30×10^{14}	32.17	-17.96

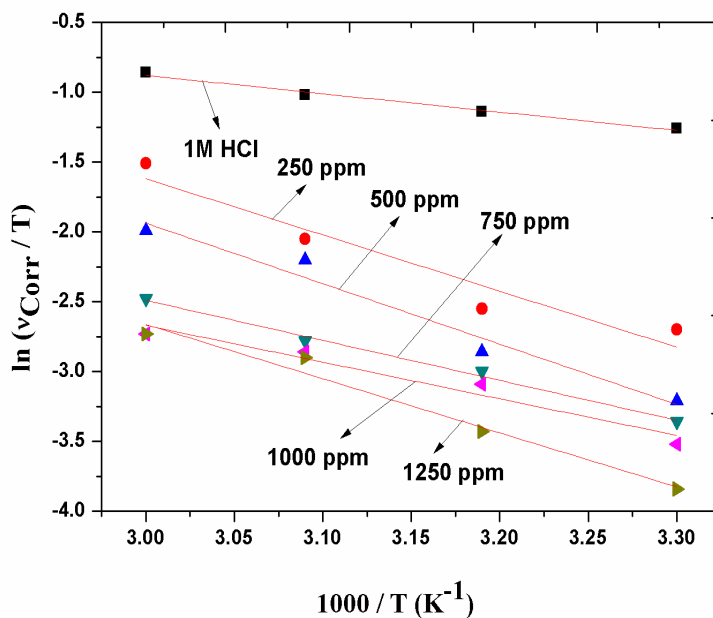


Figure 10. Transition Plot

E_a^* and A value are higher in TDF than the absence of inhibitor in 1M HCl solution. This indicated that the addition of TDF impedes metal dissolution by increasing the energy barrier for the corrosion reaction through adsorption onto metal surfaces [17]. The adsorption process resulting in a protective layer at the metal/solution interface decreases the corrosion. If the value of E_a^* for the corrosion process is greater than 20 kJ mol^{-1} in both the absence and presence of TDF in 1M HCl, it shows that the surface reaction drives the entire process.

The apparent enthalpy change (ΔH^*) and entropy change (ΔS^*) were calculated by the following Transition state equation,

$$\ln \frac{v_{Corr}}{T} = \left[\ln \frac{R}{Nh} + \frac{\Delta S^*}{R} \right] - \frac{\Delta H^*}{RT} \tag{10}$$

Where h and N are the plank's constant and Avogadro number, respectively. Graph of $\frac{v_{corr}}{T}$ against $\frac{1000}{T}$ As shown in Figure 10 with a slope of $-\Delta H^*$ and intercept of $\ln (v_{Corr}/ T)$, The calculated values of ΔH^* and ΔS^* were reported in Table 5. The positive sign of ΔH^* indicates that the reaction is endothermic for the metal dissolution process. The negative sign of ΔS^* suggests that the activation process achieved by forming an activated complex represented association during the process with a consequent loss in the degrees of freedom within the system.

3.5. SEM

The surface morphology of low carbon steel was observed by SEM measurement. Figure 11 shows that the steel surfaces immersed in the absence and presence of TDF in 1M HCl. The SEM micrograph of the low carbon steel demonstrated in 11(A) has pits and corrosive product on its surfaces. But in the presence of TDF, as in Figure 11, (B) appears as smooth and uniform surfaces, free from any corroded visibility due to the formation of a protective layer onto the metal surfaces by adsorption of the inhibitor [18]. SEM measurement indicates that TDF forms a protective layer onto the metal surfaces, resulting in reducing the corrosion.

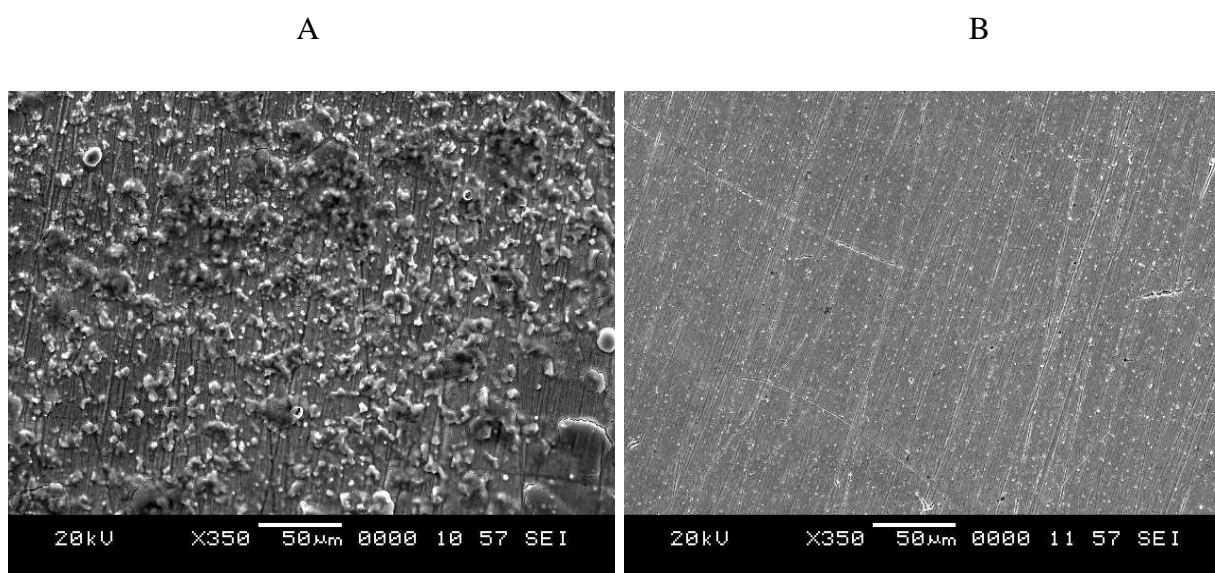


Figure 11. SEM micrographs of low carbon steel in (A) absence (B) presence of 1250 ppm of TDF in 1M HCl.

3.6 Quantum Chemical Calculations

The quantum chemical calculations are an effective technique used to explaining adsorption centres in selected inhibitor molecules through density functional theory. The optimized molecular structure of TDF is as shown in Figure 12. The energy distribution of frontier molecular orbitals (FMOs), such as highest occupied molecular orbitals (E_{HOMO}) and lowest unoccupied molecular orbitals (E_{LUMO}), are shown in Figure 13 and Figure 14, respectively.

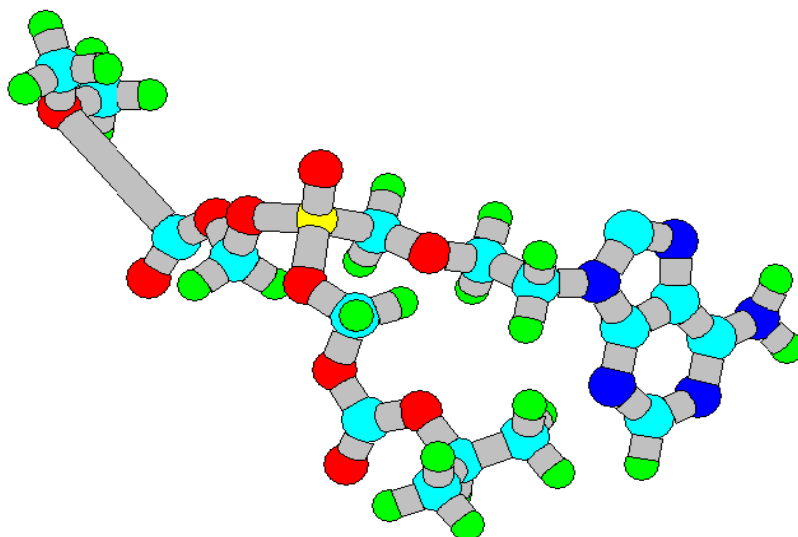


Figure 12. Optimized molecular structure of TDF

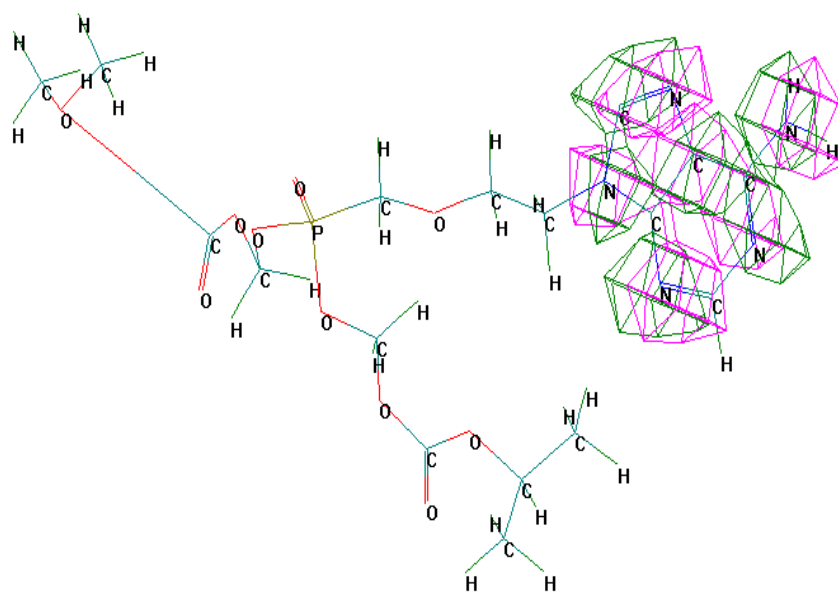


Figure 13. HOMO energy state of TDF

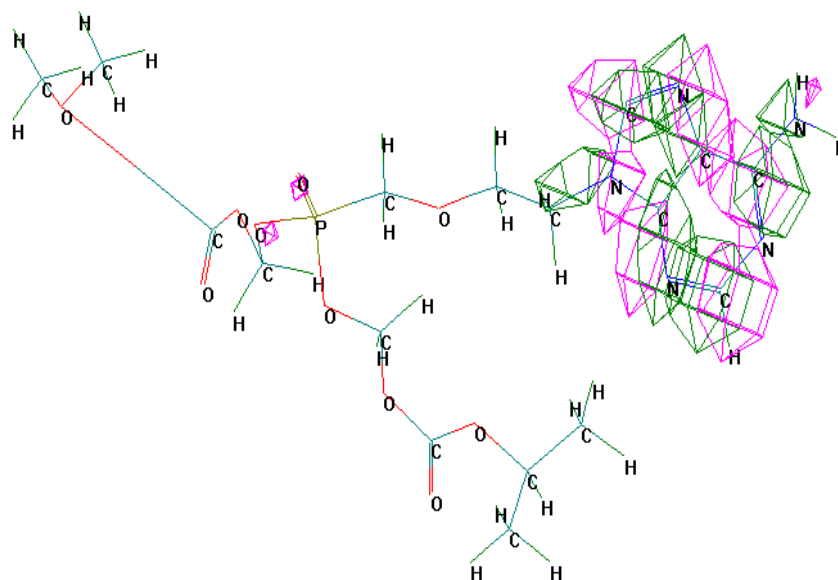


Figure 14. LUMO energy state of TDF

From density functional theory, the energy of HOMO and LUMO has significant roles in the prediction of adsorption centres in TDF molecule. The values of E_{HOMO} and E_{LUMO} are also most effective in studying the chemical interaction of the molecule. Higher the value of E_{HOMO} is having the higher electron-donating capability of the inhibitor to the metal surface, which gives a better inhibition effect. The lower the value of E_{LUMO} describes the higher the accepting ability of electrons. In this present investigation, the E_{HOMO} value of TDF is -9.30 eV, and the E_{LUMO} value is -0.86 eV. Hence, the higher the value of E_{HOMO} and lower the value E_{LUMO} , the TDF acts as a good corrosion inhibitor for low carbon steel. The energy gap ($\Delta E = E_{\text{LUMO}} - E_{\text{HOMO}}$) between HOMO and LUMO also describes an inhibitor for the metal inhibition effect. Earlier research already proved that the inhibitor having a lesser energy gap acts as a good inhibition effect for various metals. Usually, an inhibitor has a lesser ΔE value. It has high polarization, chemical reactivity, lower kinetic stability, and high adsorbing capability [19]. These imply that the inhibitor acts as a good corrosion inhibitor for metal. In our research, the TDF compound has a ΔE value of 8.44 is relatively less, while comparable with earlier research. The energy gap strongly suggested that the TDF may act as a good corrosion inhibitor for low carbon steel in 1M HCl .

Generally, the ability of a molecule that means potentiality can be described in terms of few parameters viz., Ionization potential (I), Electron affinity (A), electronegativity (χ), Global Hardness (η), and Global Softness (σ) were calculated by HOMO and LUMO energies, and their mathematical expressions are as follows,

$$\text{Ionization Potential (A)} = -E_{\text{LUMO}} \quad (11)$$

$$\text{Electron affinity (I)} = -E_{\text{HOMO}} \quad (12)$$

$$\text{Electronegativity } (\chi) = \frac{I+A}{2} \quad (13)$$

$$\text{Chemical Potential } (\alpha) = -\frac{I+A}{2} \quad (14)$$

$$\text{Global Hardness } (\eta) = \frac{I-A}{2} \quad (15)$$

$$\text{Global Softness } (\sigma) = -\frac{I-A}{2} \quad (16)$$

All calculated quantum chemical parameters for the TDF molecule were listed in Table 6

Table 6. Quantum chemical characteristics of TDF.

Sl. No.	Quantum Chemical Parameters	TDF
1	The formula of the molecule	C ₁₉ H ₃₀ N ₅ O ₁₀ P
2	Molecular Weight	287.21 g / mol
3	E _{HOMO}	-9.30 eV
4	E _{LUMO}	-0.86 eV
5	ΔE (eV)	8.44 eV
6	Dipole Moment (μ),	6.94 Debye
7	Ionization Potential, (I)	0.86
8	Electron Affinity (A)	9.30
9	Electronegativity (χ)	5.08
10	Chemical Potential (α)	-5.08
11	Global hardness (η)	-4.22
12	Global softness (σ)	4.22

The dipole moment (μ) of an inhibitor is one of the quantum chemical parameters, explain the strong interaction of inhibitor with the metal surface. Higher the value of a molecule moment suggested good chemical interaction, which results in a good inhibition effect for metal surface. TDF molecule has a high dipole moment value of 6.94 Debye while comparing with earlier researches.

Usually, a soft molecule is more reactive, and the energy difference is associated with the Softness or Hardness of the molecule. Therefore, due to the smaller energy gap and a significant-high dipole moment, the TDF is a more reactive soft molecule [20]. Thus, the TDF acts as a good corrosion inhibitor for low carbon steel in 1M HCL. Furthermore, TDF also has a high molecular weight of 287.21 g / mol and low electronegativity of 5.08 improve the adsorption capability of an inhibitor on the metal surface, which retards the corrosion. The quantum chemical calculations strengthen the experimental results and support that the TDF is a good corrosion inhibitor for low carbon steel in 1M HCl.

4. CONCLUSION

The corrosion inhibition effect of TDF for low carbon steel in 1M HCl at a temperature range of 303-333 K was studied by chemical, electrochemical, surface, and quantum chemical measurements. The inhibition efficiency of TDF increases with the increasing its concentrations. It shows more than 90 % for the optimized concentration of 1250 ppm in 1M HCl. The inhibition effect stables up to the temperature of 333 K. After that effect get decreased. The inhibition effect of TDF is attributed due to the adsorption process, which obeys the Langmuir isotherm model. Potentiodynamic polarization measurements reveal that inhibitor acts as a mixed type in nature. Adsorption studies stated that the TDF adsorption process on the metal surface is exothermic through the chemisorption spontaneously. SEM micrographs provide a visual idea about the protection from corrosion by the formation of the protective layer. The quantum parameters strengthened the experimental results and strongly recommended that the TDF act as a good corrosion inhibitor for low carbon steel in 1M HCl.

ACKNOWLEDGEMENT

The authors would like to thank the Ministry of education in Saudi Arabia and the Deanship of research at Najran University to fund this project (project number NU/ESCI/17/095). Also, the authors acknowledge the help of the Jain Institute of Technology, Davanagere.

References

1. U. M. Angst, *Mater. Struct.*, 51 (2018) 4.
2. R. Mohammadinejad R, S. Karimi, S. Irvani, R. Varma, *Green. Chem.*, 18 (2016) 20.
3. B. M. Praveen, B. M. Prasanna, N. M. Mallikarjuna, M. R. Jagadeesh, Narayana Hebbar, D. Rashmi, *Heliyon* 7 (2021) e06090.
4. Ashish Kumar Singha, Bhawna Chughb, Sourav Kr. Sahac, Priyabrata Banerjee, Eno E. Ebenso, Sanjeev Thakurb, Balaram Panie, *Results Phys.*, 14 (2019) 102383.
5. Ambrish Singh, K. R. Ansari, M. A. Quraishi, Savas Kaya, *j. mol. struct.*, 1206 (2020) 127685.
6. N. Zulfareen, T. Venugopal, K. Kannan, *Int. J. Corros.*, (2018) 9372804.
7. Chandrabhan Verma, Lukman O. Olasunkanmi, Eno E. Ebenso, M.A. Quraishi, *Results in Phys.*, 8 (2018) 657.
8. A. M. Guruprasad, H. P. Sachin, G. A. Swetha, B. M. Prasanna, *Surf. Interfaces*, 19 (2020) 100478.
9. B. M Prasanna, B. M Praveen, Narayan Hebbar, M. K Pavithra, T. S Manjunatha, R. S Malladi, *Surf. Interface Anal.*, 50 (2018) 779.
10. B. M. Praveen, B. M. Prasanna, Narayana Hebbar, P. Shivakeshava Kumar, M. R. Jagadeesh, *J. Bio. Tribo. Corros.*, 4 (2018) 1.
11. Alexandria R. C. Bredar, Amanda L. Chown, Andricus R. Burton, Byron H. Farnum, *ACS Appl. Energy Mater.*, 3 (2020) 66.
12. P. Preethi Kumari, Prakash Shetty, Suma A. Rao, *Arabian J. Chem.*, 10 (2017) 653.
13. A. K. Singh, S. Thakur, B. Pani, E. E. Ebenso, M. A. Quraishi, A. K. Pandey, *ACS Omega*, 3 (2018) 4695.
14. R. Aslam, M. Mobin, S. Zehra, I. B. Obot, E. E. Ebenso, *ACS Omega*, 2 (2017) 5691.
15. B. M Praveen, B. M Prasanna, N. M Mallikarjuna, M. R Jagadeesh, Narayana Hebbar, D. Rashmi, *Heliyon.*, 7 (2021) e06090.
16. M. Mobin, M. Rizvi, L. O. Olasunkanmi, E. E. Ebenso, *ACS Omega*, 2 (2017) 3997.

17. Amrita Biswas, Sagar Pal, G. Udayabhanu, *J. Adhes. Sci. Technol.*, 31 (2017) 2468.
18. Deepa Prabhu, P. R. Prabhu, Padmalatha Rao, *Chem. Pap.*, 75 (2020) 653.
19. Omar Fergachia, Fouad Benhibae, Mohamed Rbaab, Rachid Touira,d, Moussa Ouakkic, Mohsine Galaia, Brahim Lakhressib, Hassan Ouddae, Mohamed Ebn Touhamia, *Mater. Res.*, 21 (2018) e20171038.
20. A. S. Fouda, H. S. El-Desoky, M. A. Abdel-Galeil, Dina Mansour, *SN Appl. Sci.*, 3 (2021) 287.

© 2021 The Authors. Published by ESG (www.electrochemsci.org). This article is an open access article distributed under the terms and conditions of the Creative Commons Attribution license (<http://creativecommons.org/licenses/by/4.0/>).